Photothermal Therapeutic Response of Cancer Cells to Aptamer–Gold Nanoparticle-Hybridized Graphene Oxide under NIR Illumination

Lingyan Yang,[†] Yu-Ting Tseng,[‡] Guangli Suo,[†] Liliang Chen,[§] Jiantao Yu,[†] Wei-Jane Chiu,[∥] Chih-Ching Huang,*[,∥,⊥,#] and Chia-Hua Lin*[,†]

[†]Key Laboratory of Nano-Bio Interface, Suzhou Key Laboratory for Nanotheranostics, Division of Nanobiomedicine, Suzhou Institute of Nano-Tech and Nano-Bionics, Chinese Academy of Sciences, Suzhou 215123, China

[‡]Department of Chemistry, National Taiwan University, Taipei, 10617, Taiwan

[§]The National Key Laboratory of Shock Wave and Detonation Physics, Institute of Fluid Physics, CAEP, Mianyang 621900, China

[∥]Department of Bioscience and Biotechnology, National Taiwan Ocean University, Keelung, 20224, Taiwan

[⊥]Center of Excellence for the Oceans, National Taiwan Ocean University, Keelung, 20224, Taiwan

[#]School of Pharmacy, College of Pharmacy, Kaohsiung Medical University, Kaohsiung, 80708, Taiwan

Ⓢ *Supporting Information*

ABSTRACT: The objective of this study was to synthesize a nanocomposite, aptamer–gold nanoparticle-hybridized graphene oxide (Apt-AuNP–GO), to facilitate targeted treatment of tumor cells by near-infrared (NIR) light-activatable photothermal therapy. We also investigated whether Apt-AuNP–GO with NIR illumination modulates heat shock proteins (HSPs) expression leading to therapeutic response in human breast cancer cells. These findings can provide

strategies for improving the photothermal therapy efficacy of cancer. The self-assembled Apt-AuNP–GO nanocomposite could selectively target MUC1-positive human breast cancer cells (MCF-7) due to the specific interaction between the MUC1-binding-aptamer and the MUC1 (type I transmembrane mucin glycoprotein) on cell membrane. In addition, Apt-AuNP–GO has a high light-to-heat conversion capability for photoabsorption of NIR light, and it is able to exert therapeutic effects on MCF-7 cells at an ultralow concentration without inducing adverse effects in healthy cells. The Apt-AuNP–GO nanocomposites combine the advantages of GOs, AuNPs, and Apts, possess specific targeting capability, excellent biocompatibility, and tumor cell destruction ability, suggesting great potential for application in the photothermal therapy of breast cancer. Under NIR illumination, Apt-AuNP–GO induced transient increase in HSP70 expression, which decreased thereafter. This phenomenon may cause irreversible damage to Apt-AuNP–GO-treated MCF-7 cell under NIR illumination. We also demonstrated that the combination therapy of heat and HSP70 inhibitor could synergistically generate marked tumoricidal effects against breast cancer. These results suggest that the degree and duration of HSP70 protein expression are correlated with therapeutic effects against breast cancer for Apt-AuNP–GO-assisted photothermal therapy. We believe that such a nanocomposite can be readily extended to the construction of HSP70 inhibitors-loaded Apt-AuNP–GO, which could deliver both heat and HSP70 inhibitors to tumorigenic regions for the chemo-photothermal therapy.

KEYWORDS: graphene oxides, gold nanoparticles, aptamers, phototherapy, cancer cells, HSP70
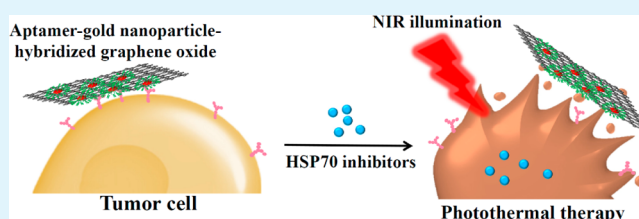
1. INTRODUCTION

Breast cancer is a leading cause of death among women worldwide. According to statistics reported by the International Agency for Research on Cancer (IARC), the incidence of breast cancer has increased by more than 20%, while mortality has increased by 14% since 2008. Breast cancer is also the most common cause of cancer death and the most frequently diagnosed cancer among women.[1,2] Continuous improvements in the techniques for curing breast cancer, understanding the related mechanisms, and the development of new medicines will result in more efficient and effective cancer treatment.

Recently, the application of nanotechnology for cancer therapy has received extensive attention. Nanotechnology-related cancer treatment would involve the use of nanomaterials that can be conjugated with specific molecules, such as imaging reporters, antibodies, and anticancer drugs, to improve the efficiency and safety of therapy.[3−12] Photothermal therapy is a noninvasive cancer therapy technique in which tumor tissues are exposed to light, and the received light is converted

to heat to promote tumor destruction. Photothermal therapy involves raising the temperature of tumor cells to the range of 42−46 °C to alter the function of many structural and enzymatic proteins within cells, thereby leading to cell death.[13,14] Several nanomaterials with optical absorption in the near-infrared (NIR) spectrum, such as gold nanoparticles (AuNPs), iron oxide nanoparticles, graphene oxides (GOs) and carbon nanotubes, have been developed for the photo-hyperthermic treatment of cancer.[15−18] These nanomaterials have attracted much attention because normal tissues are transparent in the NIR region. NIR (700−1000 nm) irradiation is the most advantageous wavelength region suitable for biological applications owing to its high capability of deeper penetration into animal tissues in this optical window.

GOs and AuNPs have been extensively employed in photothermal therapy because of their excellent photothermal conversion efficiencies and biocompatibilities.[19−21] Further enhancement of the photothermal efficiency of these two materials generally requires control of their oxidation states, morphologies, or dimensions.[19−21] Recently, a number of recent studies have demonstrated that the Au materials anchored on GO could enhance the photothermal effects and control the shape and size of the gold nanostructures could tune the photothermal effects. In addition, GOs are excellent nanomaterials as drug carriers due to their high loading capacity.[22,23] Therefore, creating a nanomatrix by combining GOs with AuNPs in a single system may enhance the photothermal effects on tumors.

The major challenge in photothermal therapy is controlling the highly localized thermal effects on tumor. Over the past few years, many researchers have developed aptamers to replace antibodies in medical use such as in disease diagnosis, drug delivery, and therapeutics.[3,24,25] With their advantages of simple synthesis methods, small sizes, and ease of modification and storage, aptamers are widely employed for specific targeting of cancer cells.[3,26] To provide a nanomatrix with the targeting capability for specific human breast cancer cells, we immobilized mucin 1 (MUC1) aptamers on the surface of the nanomatrix. MUC1 is a well-characterized transmembrane glycoprotein whose expression increases in most breast malignant carcinomas.[3,27,28] Several studies have demonstrated that MUC1 overexpression is linked to tumor aggressiveness in human breast carcinoma.[29,30] These findings suggest that MUC1 can act as a target in breast cancer therapy. Here, we constructed an aptamer-guided AuNP-GO for photothermal therapy of MUC1-positive breast cancer cells (MCF-7). Furthermore, to increase the binding efficiency of MUC1 aptamers on this nanomatrix, MUC1 aptamers were first conjugated to AuNPs via a strong Au−S bond and then adsorbed onto GO. To explore the therapeutic efficiency of our photothermal agent, we evaluated its therapeutic effect and delivery capacity in human breast cancer cells.

The efficiency of thermal therapy can frequently be reduced because of the induction of heat shock proteins (HSPs). HSPs, such as HSP70 and HSP90, can help protect cells from heat stress and maintain homeostasis.[31−33] HSPs can be rapidly activated once heat stress occurs, which allows them to effectively protect against heat-induced toxicity.[34−36] Therefore, overcoming the resistance of HSPs can help advance the potential of cancer thermal therapy. Numerous studies have demonstrated that cotreatment of cancer cells with hyper-thermia and HSP90 inhibitors is a powerful approach for improving cancer therapy.[37−39] However, the overexpression of HSP70 following treatment with HSP90 inhibitors, which reduces anticancer efficacy, has been demonstrated in vitro and in vivo.[40−43] Therefore, to clarify the HSP expression induced by photothermal therapy alone or in combination with HSP inhibitors might help to improve the efficiency of this form of cancer therapy.

In this study, we developed Apt-AuNP−GO, which can deliver heat to specific tumorigenic regions to effectively inhibit human breast cancer cell growth by inducing apoptosis at ultralow concentrations. The results of our study show that the Apt-AuNP−GO displayed excellent anticancer activity, specific targeting capability and biocompatibility, suggesting great potential for application as a photothermal agent. We also examined the possible involvement of HSP70 in the heat stress response that induced by Apt-AuNP−GO on human breast cancer cells. We therefore utilized the HSP70 inhibitor (VER-155008) to validate the proposed therapeutic approach. These results provide the biological basis for drug designs and breast cancer treatments.

2. EXPERIMENTAL SECTION

2.1. Chemicals. Bisbenzimide Hoechst 33342, thiazolyl blue tetrazolium bromide (MTT) and 5′-O-[(4-cyanophenyl)methyl]-8-[[(3,4-dichlorophenyl)methyl]amino]− adenosine (VER-155008) were purchased form Sigma-Aldrich (Milwaukee, WI). RPMI 1640 with 1% L-glutamine, phosphate buffered saline (0.01 M, pH 7.2) and fetal bovine serum were purchased form Gibco (Life Technologies, Thermo Fisher Scientific, Waltham, MA). HSP70 antibody, HSP90 antibody, HRP-labeled goat anti-rabbit IgG, HRP-labeled goat anti-mouse IgG, Alexa Fluor 488-labeled goat anti-rabbit IgG, lactate dehydrogenase (LDH) cytotoxicity assay kit were purchased form Beyotime Institute of Biotechnology (Shanghai, China). All other chemicals were purchased from Sigma-Aldrich, Abcam (Cambridge, MA), or Epitomics (Burlingame, CA), unless stated otherwise, and used without further purification.

2.2. Cell Cultures. The human breast cancer MCF-7 cells and human umbilical vein endothelial EA.hy926 cells were maintained in RPMI 1640 with 10% fetal bovine serum in a 37 °C incubator with a humidified mixture of 5% CO_2 and 95% air. The medium was changed twice a week, and the cells were passaged by trypsinization every week.

2.3. Temperature Monitoring of Laser-Induced Heat Generation. Nanoparticle suspensions in cell culture medium were illuminated with an 808 nm NIR laser. The real-time temperature elevations were measured using thermocouple. To examine the potential of using Apt-AuNP−GO in photothermal therapy, hybrid nanomaterials suspension in cell culture medium was added into the MCF-7 or EA.hy926 cells (8000 cells/well), cultured for 24 h, and then rinsed three times with PBS to remove any free Apt-AuNP−GO. The samples were illuminated with an 808 nm NIR laser with the power density of 3 W for 5 min. The potential of nanoparticles in photothermal therapy was then assessed at 3, 12, and 24 h after NIR laser illumination by MTT and LDH assay.

2.4. Targeting-Ability of Apt-AuNP−GO Nanocomposites. To examine the targeting-ability of Apt-AuNP−GO, fluorescence agent, rhodamine B (RB; 500 nM), was loaded onto GO, random single-stranded DNA-AuNP−GO or Apt-AuNP−GO, and then the unbound RB was removed together with in the supernatant after centrifugation at a RCF of 35 000g for 1 h. After removing the supernatant, the pellet of RB/nanoparticles was resuspended in PBS solution. The cell culture medium containing RB/nanoparticles (1.74 μg/mL) was separately added into the MCF-7 and EA.hy926 cells for 24 h, and then rinsed three times with PBS to remove any free RB/nanoparticles. The fluorescent images of RB/nanoparticles targeting cells were recorded with a fluorescence microscope (Eclipse Ti, Nikon, Melville, NY,) and flow cytometry (Accuri C6, BD Biosciences, San Jose, CA). To determine the cellular uptake of nanocomposites, MCF-7 cells were exposed to Apt-AuNP−GO for 24 h and analyzed by

Scheme 1. Schematic Representation of the Preparation of Apt-AuNP−GO and Its Application with NIR Laser Irradiation for Photothermal Therapy of Cancer Cells
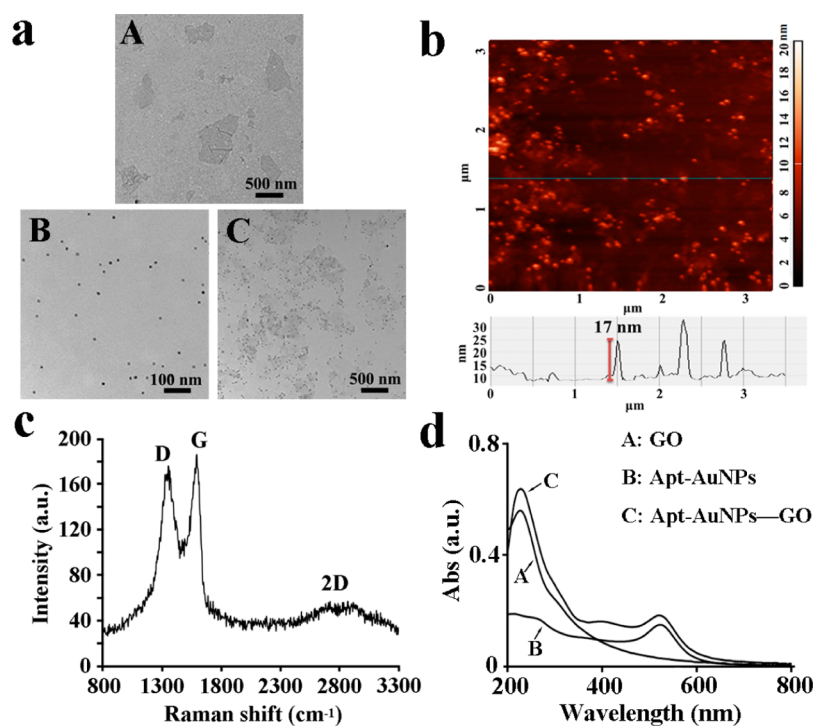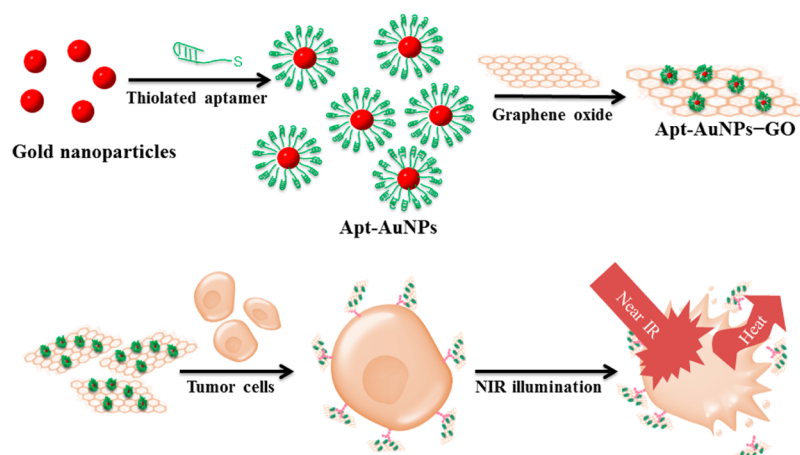

Figure 1. Physicochemical properties. (a) TEM images of as-prepared (A) GO, (B) Apt-AuNPs, and (C) Apt-AuNP−GO. (b) Tapping mode AFM image of Apt-AuNP−GO. (c) Raman spectra of the prepared GO. (d) UV−vis absorption spectra of (A) GO (at a concentration of 2×), (B) Apt-AuNPs (0.5 nM), and (C) Apt-AuNP−GO (prepared from 2× GO and 0.5 nM Apt-AuNPs) in sodium phosphate solution (5 mM, pH 7). The absorbance (Abs) is plotted in arbitrary units (a.u.).

TEM. The MCF-7 cells were washed with PBS and fixed in 1% OsO_4. The cells were dehydrated with an ethanol gradient and immersed in LR white resin for 24 h at 60 °C. The cells were subsequently embedded in an epoxy resin, and then a thin section was sliced using a diamond microtome. Each slice was mounted on TEM grid and stained with uranyl and lead acetate, air-dried, and imaged under TEM.

2.5. Cell Viability. Cells were treated with GO, Apt-AuNP, Apt-AuNP−GO or NIR illumination alone or in combination. Cell viability was determined with the MTT and LDH assays according to the manufacturer's protocol. The samples were determined by a spectrophotometer (Victor X4, 2030 Multilabel Reader, PerkinElmer) and compared with the values of controls. Visible absorbance was recorded in a 96-well plate reader at 490 nm. The cell viability was expressed as the absorbance percentage relative to that of control group.

2.6. Apoptosis-Related and HSPs Protein Expression. Levels of Bax, Bcl2, HSP70, and HSP90 proteins were determined by Western blot analysis. MCF-7 cells were treated with VER-155008, 17-AAG, GO, Apt-AuNP−GO or NIR illumination alone or in combination. After the treatment, cells were washed three times with PBS, centrifuged at 8000g for 5 min, and were soaked in liquid N_2. Cell pellets were thawed and lysed in 80 μL of protein extraction buffer (1 M Tris-HCl, pH 7.9, 3 M NaCl, 1% aprotinin, 2 mM phenylmethylsulfonyl fluoride, 5 mM dithiothreitol) for 30 min on ice, and the extracts were centrifuged for 30 min at a RCF of 10 000 g. Protein concentration was measured with the Bio-Rad protein assay kit (Hercules, CA). Protein were loaded at 50 μg/lane and separated by 12% (w/v) sodium dodecyl sulfate-polyacrylamide gel electrophoresis and blotted. Anti-Bcl2, anti-Bax (ImmunoWay Biotechnology Company, Newark, DE), anti-HSP70, anti-HSP90, and anti-β-actin
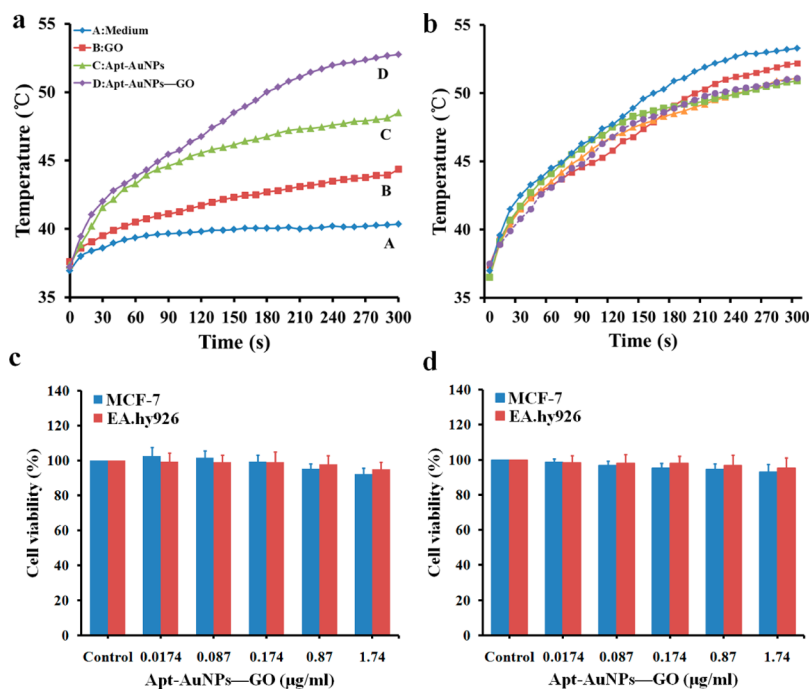
Figure 2. Photothermal effects and cytotoxicity of Apt-AuNP−GO. (a) Photothermal heating curve of (A) RPMI1640 medium as a control, (B) GO (1.74 μg/mL), (C) Apt-AuNPs (0.2 nM), and (D) Apt-AuNP−GO (1.74 μg/mL). (b) Photothermal stability (five consecutively repeated cycles) of Apt-AuNP−GO (1.74 μg/mL) under NIR illumination. Cytotoxicity of Apt-AuNP−GO (0.0174−1.74 μg/mL in RPMI 1640 medium) was measured by (c) MTT assay and (d) LDH assay.

monoclonal antibodies were used at a concentration of 1:1000. The secondary antibodies, alkaline phosphatase-coupled antimouse or antirabbit antibody were incubated at room temperature for 2 h at a concentration of 1:1000 dilutions, respectively. Immunoreactive bands were visualized by incubating with ECL Plus Substrate (Pierce, Thermo Scientific, Waltham, MA). The membranes were also probed with anti-β-actin antibody to correct for differences in protein loading.

2.7. Statistical Analysis. Comparison of the results between various experimentally treated groups and their corresponding controls was carried out by Student t-test. All comparisons were considered significantly different when *$p < 0.05$.

Please see the Supporting Information for the details on the preparation of GO nanosheets, preparation and characterization of Apt-AuNP and Apt-AuNP−GO, photothermal conversion efficiency of Apt-AuNP−GO and reduced GO (rGO), and agarose gel separation of the mixtures of Apt−AuNP and GO.

3. RESULTS AND DISCUSSION

3.1. Preparation of Apt-AuNP−GO and RB/Apt-AuNP−GO. Scheme 1 outlines the synthesis route for the preparation of Apt-AuNP−GO hybrid nanomaterials. First, GO was synthesized from graphite (7−11 μm) using a modified Hummers method.[44] TEM study showed that the average sizes of the single-layer GOs were approximately 300 nm (Figure 1a,A). The Raman spectra of the as-prepared GO showed the specific band associated with the in-phase vibration of the graphene lattice (G band, sp^2) at 1575 cm^{-1} as well as the disorder band associated with graphene edges (D band, sp^3) at approximately 1355 cm^{-1} (Figure 1c).[45] As-prepared GO at a concentration of 1× (where the concentration of as-prepared GO is denoted by 100×) and Apt-AuNP (10 nM; 13 nm) in a sodium phosphate solution (5 mM; pH 7.0) were used to prepare Apt-AuNP−GO. Approximately 98% of the Apt-AuNP was determined to be adsorbed onto the GO by comparing the absorbance values at 520 nm of the Apt-AuNP in standard solution and in the supernatant after centrifugation (at a RCF

of 5000g for 10 min) of the Ap-AuNP/GO mixture. Apt-AuNP were adsorbed on GO mainly through multivalent nucleobase−graphene π−π stacking (attractive, noncovalent interactions between aromatic rings through the π electrons) between the aptamers and GO. The high density of aptamer units on AuNP resulted in the strong cooperative π−π stacking interaction between Apt-AuNPs and GO.[46] The TEM image (Figure 1a,C) and the result of agarose gel separation (Figure S1, Supporting Information) of Apt-AuNP−GO reveal that the Apt-AuNP were assembled homogeneously on the GO surface. The atomic force microscope (AFM) image and UV−vis absorption spectra of Apt-AuNP−GO shown in Figure 1b,d further confirm that the AuNPs were well distributed on the surface of each GO. The GO shows a $\pi \rightarrow \pi^*$ transition of the C=C bond in the sp^2 hybrid region at 230 nm and a shoulder of n → π^* electronic transition of peroxide and/or epoxide functional groups at approximately 300 nm.[47] Both spectra of Apt-AuNP and Apt-AuNP−GO spectra show an absorption band at 520 nm, which was attributed to the dispersed AuNPs (13 nm).[48] Based on simple π−π stacking and electrostatic interactions between rhodamine B (RB) and GO, we prepared fluorescent RB-modified Apt-AuNP−GO (RB/Apt-AuNP−GO) for selective cell targeting. We observed the quantum yield of RB (30%) decreased to ∼5% after being adsorbed on Apt-AuNP−GO as a result of energy and electron transfer between RB and the GO (data not shown).[49]

3.2. Photothermal Effects and Cytotoxicity Assessment of Apt-AuNP−GO. In previous studies, functional GO was used for effective photothermal tumor therapy under NIR illumination due to its high NIR absorption.[50,51] To examine the photothermal heating capabilities of GO nanosheets, Apt-AuNPs, and Apt-AuNP−GO nanocomposites, we detected the temperature variation of RPMI 1640 cell medium solution (100 μL) containing GO (1.74 μg/mL), Apt-AuNPs (0.2 nM), or
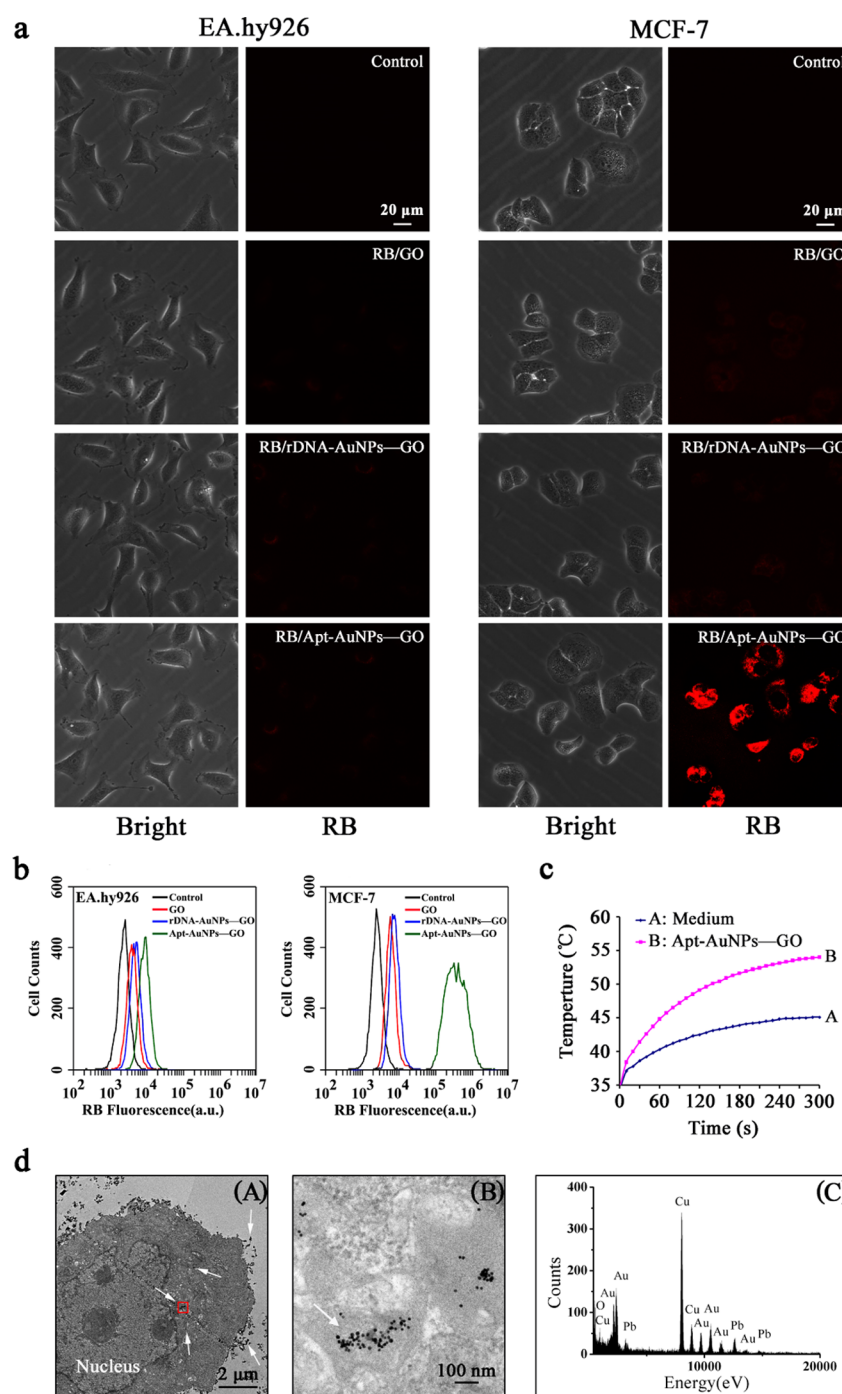
Figure 3. Targeting ability and selective photothermal capability. (a) Fluorescence image of MCF-7 and EA.hy926 cells incubated with RB/GO, RB/rDNA-Au NPs—GO, and RB/Apt-AuNP—GO (1.74 μg/mL in RPMI1640 medium). (b) Fluorescence intensity MCF-7 and EA.hy926 cells incubated with RB/GO, RB/rDNA-Au NPs—GO, and RB/Apt-AuNP—GO (1.74 μg/mL in RPMI 1640 medium). (c) Selective photothermal heating capability of Apt-AuNP—GO (1.74 μg/mL in RPMI 1640 medium). (d) Uptake of Apt-AuNP—GO by MCF-7 cell. (A) TEM images of MCF-7 cells exposed to Apt-AuNP—GO for 24 h. White arrows denote Apt-AuNP—GO, (B) higher magnification of MCF-7 cells (red boxed area in image A), and (C) EDX pattern of the Apt-AuNP—GO in MCF-7 cells (white arrows in image B).

Apt-AuNP—GO (1.74 μg/mL) after exposed to an 808 nm NIR laser at power density of 3 W using a thermocouple. As shown in Figure 2a, the temperature of the GO solutions increased by 1.3 °C/min (curve B; from 37.6 to 44.3 °C over 5 min). The temperature of the Apt-AuNPs solutions increased by 2.2 °C/min (curve C; from 37.4 to 48.5 °C over 5 min). The temperature of the Apt-AuNP—GO solutions showed greater changes, increased by 3.1 °C/min (curve D; from 37.2 to 52.8 °C over 5 min). In contrast, the cell culture medium, used as the control group, exhibited only a slight increase in temperature (curve A; 0.7 °C/min, from 37.0 to 40.4 °C over 5 min). A promoting effect was observed to be responsible for the temperature elevation of the Apt-AuNP—GO (Figure 2a), which might be attributed to both light absorption by GO and plasmonic effects associated with the Apt-AuNPs.[52] The spherical AuNPs with small size tend to deposit on defect
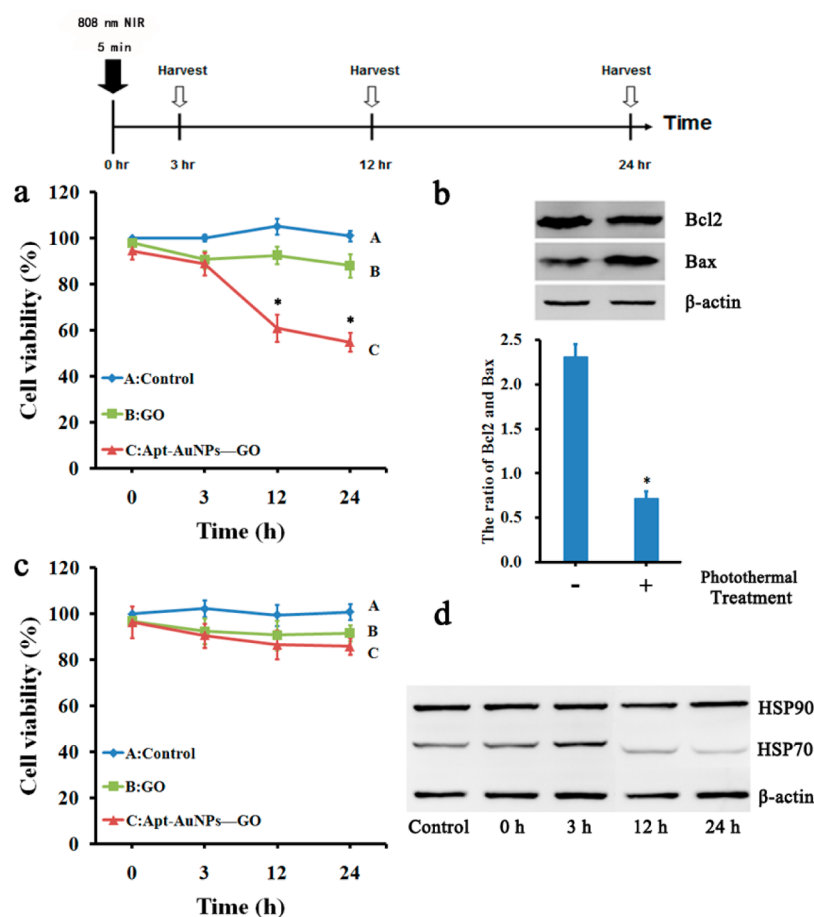
Figure 4. Photothermal therapy effect. (a) Cell viability of MCF-7 cells was measured by MTT assay 3−24 h after incubation with Apt-AuNP−GO (1.74 μg/mL), GO (1.74 μg/mL), and RPMI 1640 medium as a control under NIR illumination. (b) Western blot method to measure the Bax and Bcl2 protein expression in MCF-7 cells at 24 h after treatment of GO or Apt-AuNP−GO (1.74 ug/mL in RPMI 1640 medium) coupled with NIR illumination. (c) Cell viability of EA.hy926 cells was measured by MTT assay at 3−24 h after incubation with Apt-AuNP−GO (1.74 μg/mL), GO (1.74 μg/mL) and RPMI 1640 medium as a control and coupled with NIR illumination. (d) Western blot images of HSP70 and HSP90 expression in MCF-7 cell after treatment of Apt-AuNP−GO (1.74 μg/mL in RPMI 1640 medium) coupled with NIR illumination. (*$P < 0.05$).

sites and vacancies of GO and thus decrease the mobility of the AuNPs on GO after absorbing laser energy, therefore, it limits their shape transformation and shows efficient laser energy conversion. Recently, Abdelsayed et al. have reported the laser illumination of GO results in a rapid deoxygenation accompanied by an increase in thermal conductivity, and further enhancement of heat-transfer process.[53] We suggest the features of catalytic AuNPs may accelerate the deoxygenation of GO and improve the photothermal conversion efficiency of AuNP−GO nanocomposite.[7] To assess the NIR photostability of Apt-AuNP−GO, five laser-on/off cycles were performed by irradiating the cell culture medium containing Apt-AuNP−GO via an 808 nm laser for 5 min (laser-on), followed by cooling to room temperature without laser irradiation for 5 min (laser-off). As shown in Figure 2b, no significant variation was observed during photothermal heating after five cycles. The TEM images, UV−vis absorption spectra, and Raman spectra of Apt-AuNP−GO in PBS solution after NIR illumination were almost the same as that of untreated one, revealing the dispersibility and structure of the Apt-AuNP−GO remained unchanged after NIR illumination (Figure S2, Supporting Information). These results also suggest that the Apt-AuNPs did not release from GO under the NIR illumination. The gel separation results shown in Figure S1 (Supporting Informa-

tion) further support the Apt-AuNP−GO nanocomposites were stable (no aggregation) and Apt−AuNPs did not release from GO after NIR illumination. The high stability of the Apt-AuNP−GO is consistent with previous results obtained for graphene-based materials with similar temperature profiles in recycling tests.[17,53]

To further evaluate the biocompatibility of Apt-AuNP−GO, we measured the viability of human breast cancer cells (MCF-7) and human vascular endothelial cells (EA.hy926) after treatment with Apt-AuNP−GO (0.0174−1.74 μg/mL). Numerous studies have demonstrated that nanomaterials may potentially affect the results of cytotoxicity assays due to their high adsorption capacity and optical activity.[54] To prevent false evaluations of cell viability, both MTT and LDH assays were used to assess cytotoxicity. As shown in Figure 2c,d, the viability of both MCF-7 and EA.hy926 cells remained above ∼95%, even after incubation with the Apt-AuNP−GO for 24 h. Inclusion of Apt-AuNP−GO did not cause cytotoxicity, demonstrating the inherent toxicity of GO hybridized with Apt-AuNPs in selected cell lines are quite low. Overall, our results suggested that Apt-AuNP−GO can serve as a biocompatible material for photothermal therapy of cancer, exhibiting an excellent NIR photothermal energy conversion function and stability.

3.3. Targeting Ability and Selective Photothermal Capability of Apt-AuNP−GO. To achieve a highly localized thermal effect on breast tumor cells, we used surface-immobilized MUC1 aptamers to specifically target MUC1-positive breast cancer cells. First, we evaluated the expression of MUC1 membrane proteins in MCF-7 cells and EA.hy926 cells by immunolabeling and immunoblot analysis. Our results indicate that only MCF-7 is MUC1-positive cell line (Figure S3, Supporting Information).[29,30] To further investigate the targeting ability of Apt-AuNP−GO, RB molecules were loaded onto Apt-AuNP−GO to form fluorescent RB/Apt-AuNP−GO. As shown in Figure 3a, after being treated with RB/Apt-AuNP−GO (1.74 μg/mL) for 24 h, EA.hy926 cells showed very weak fluorescence. In contrast, RB emitted strong red fluorescence, indicating that the RB/Apt-AuNP−GO has bound to the surface of MCF-7 cells. We also evaluated the binding specificity of GO, random single-stranded DNA-gold nanoparticle-hybridized graphene oxide (rDNA-AuNP−GO) to MCF-7 and EA.hy926 cells. Both MCF-7 and EA.hy926 cells showed very weak fluorescence after treated with RB/rDNA-AuNP−GO for 24 h (Figure 3a). In addition, flow cytometry analysis indicated that a significant increase in fluorescence intensity was observed in MCF-7 after labeling with RB/Apt-AuNP−GO, but not in EA.hy926 cells (Figure 3b). We also studied the selective photothermal heating effect of Apt-AuNP−GO. As shown in Figure 3c, the temperature of medium in Apt-AuNP−GO-treated MCF-7 cells were significantly increased to ∼53 °C after continuous irradiation by NIR for 5 min. Our results demonstrate that Apt-AuNP−GO can selectively target MUC-1 positive cells (Figure 3). We also tested the labeling of Apt-AuNP−GO to another MUC1-postive breast cancer cell line (T47D cell). Our result (Figure S4, Supporting Information) indicated RB/Apt-AuNP−GO exhibits similar labeling efficiency for T47D cells when compared to MCF-7 cells. The Apt-AuNP−GO nanocomposites possess highly specific targeting capability to MUC1-positive cancer cells. Therefore, we expect the damage of normal cells was very low when using Apt-AuNP−GO nanocomposites coupled with NIR illumination for targeted photothermal therapy of tumors. The whole surfaces of AuNPs were modified by aptamer molecules through Au−S bond to form three-dimensional-like spherical aptamer-AuNP conjugates. In this study, the AuNPs (∼13 nm) were capped with MUC1-binding-aptamer ligand with high density on its surface (∼70 aptamer molecules per AuNP). The aptamer molecules on the AuNPs that are opposite to aptamer-GO interaction side retain their targeting ability to MUC1 proteins on cell membranes. The ultrahigh aptamer density on the AuNP−GO nanocomposites and the high local concentration of flexible aptamer ligands enhance the cooperative binding affinity for MUC1 on the cell membrane. Furthermore, the Apt-AuNP−GO bound to the MUC-1 protein was then internalized by MCF-7 cells. Most of the Apt-AuNP−GO was confined to cytoplasm and did not enter the nucleus (Figure 3d). The nanosheet structure of GO enables easy adhesion on the plasma membrane and high uptake by mammalian cells through endocytosis[55] may contribute to the strong affinity of Apt-AuNP−GO for human cancer cells. Accordingly, Apt-AuNP−GO can be a potential drug carrier to carry antitumor drugs into cell for breast cancer therapy. Our results revealed that Apt-AuNP−GO exhibited both excellent tumor targeting and photothermal heating properties toward MCF-7 breast cancer cells.

3.4. Photothermal Therapy Effect and Bio-Safety of Apt-AuNP−GO. After demonstrating the specific capture of MCF-7 cells by Apt-AuNP−GO, we performed NIR illumination experiments to evaluate whether Apt-AuNP−GO can be used for photothermal therapy of MCF-7 breast cancer cells. To examine the photothermal therapeutic response, MCF-7 cells were treated with Apt-AuNP−GO or GO (1.74 μg/mL) for 24 h. After removing the nonbinding Apt-AuNP−GO or GO, the cell cultures were irradiated by NIR for 5 min. The cells were then incubated again at 37 °C for 3, 12, and 24 h before determining the viability of MCF-7 cells by an MTT assay. The results showed that Apt-AuNP−GO induced more significant therapeutic effects than GO in MCF-7 cells (Figure 4a). In addition the relative MCF-7 cell viability decreased continuously over time after treating with Apt-AuNP−GO and NIR illumination (Figure 4a). This result suggests that photothermal therapy induced by Apt-AuNP−GO led to irreversible and serious damage to MCF-7 cells. To further examine whether Apt-AuNP−GO coupled with NIR illumination induces cell death by apoptosis, we conducted a Western blot analysis of apoptosis regulatory proteins, including Bax and Bcl2. The decrease in the Bcl2/Bax ratio suggested Apt-AuNP−GO coupled with NIR illumination induce apoptosis in MCF-7 cells (Figure 4b). The induction of apoptosis in target MCF-7 cells may be a better approach to cancer therapy because it will not induce inflammation which may cause further distress or injury within normal cells.[56]

To evaluate the biosafety of the photothermal therapy by using Apt-AuNP−GO nanocomposites, we examined the cytotoxic effect of EA.hy926 cells by using the same treatment regime applied to MCF-7 cells. An MTT assay was also performed to evaluate the cytotoxicity of EA.hy926 cells following photothermal therapy. As shown in Figure 4c, Apt-AuNP−GO did not induce any significant cytotoxic effects in EA.hy926 cells because Apt-AuNP−GO could not bind to MUC1-negative EA.hy926 cells. Our Apt-AuNP−GO possesses several unique properties and functionalities, such as stability, excellent light−heat conversion efficiency, tumor-targeting properties and biosafety, which make it an ideal photothermal agent for therapy of MUC1-overexpressing cancers.

It has been demonstrated that HSPs can act as key regulators in the apoptosis pathway to prevent unintended cell death induced by a given stress.[57] Therefore, exploring the role of HSPs (HSP70/90) in photothermal therapy and overcoming the resistance of HSPs can help advance the potential of cancer thermal therapy. As shown in Figure 4d, HSP70 expression increased after 5 min of NIR irradiation, reaching a highest level at 3 h, and decreased thereafter. It appears that the MCF-7 cells tried to increase their HSP70 expression in the compensatory stage (3 h). Once it was established that HSP70 could not completely remove heat-induced damaged proteins, it was determined that the MCF-7 cells had entered the decompensatory stage (12 and 24 h) with reduced HSP70 expression, which in turn induced irreversible damage to MCF-7 cells (Figure 4a). However, we did not observe a significant change in HSP90 expression relative to the expression level measured for the control (β-actin) because HSP90 was expressed constitutively and abundantly in MCF-7 cells (Figure 4d).[37] Our findings reveal that HSP70 protein expression is a vital heat-response protein in photothermal therapy of breast cancer cells. Therefore, HSP70 inhibitors may be considered promising compounds for promoting photothermal therapy of breast cancer.

3.5. HSPs Expression and Synergistic Effect of Photothermal Therapy and HSPs Inhibitors. Numerous studies have reported that overexpression of HSPs is correlated with the therapeutic resistance of cancer cells.[37−39] Neutralization of HSPs is therefore an attractive strategy for enhancing the photothermal therapeutic effects of cancer cells. However, treatment with an HSP90 inhibitor strongly induces HSP70 expression, reducing the efficiency of photothermal therapy.[34,40,41] Therefore, clarifying the compensatory effects of HSPs inhibitors in MCF-7 cells is a critical step for promoting the therapeutic efficiency of combined photothermo/chemotherapy. To examine the compensatory effects, MCF-7 cells were treated with Apt-AuNP−GO or GO (1.74 μg/mL) for 24 h. After removing the nonbinding Apt-AuNP−GO or GO, the HSPs inhibitors-free and HSPs inhibitors-containing cell cultures were irradiated by NIR for 5 min. As shown in Figure 5a, HSP70 inhibitor (VER-155008, 1 μM) did not induce any
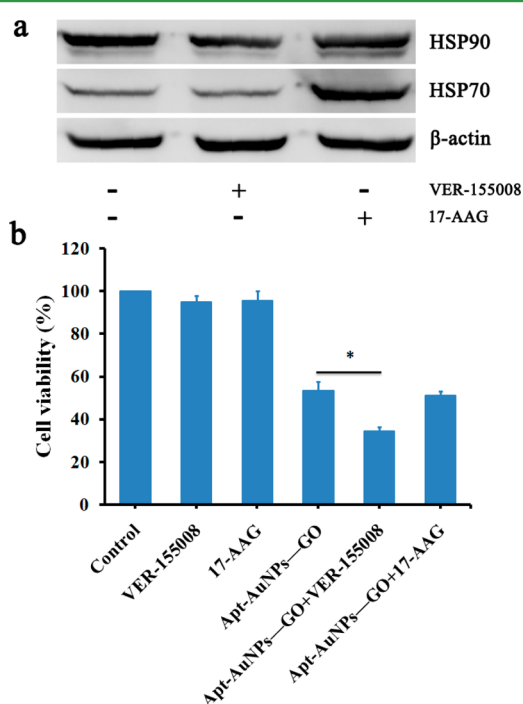

Figure 5. HSP70/90 expression and synergistic effect of photothermal therapy and HSP70/90 inhibitor. (a) Western blot images of HSP70 and HSP90 expression in MCF-7 cell 24 h after incubated with HSP70 inhibitor (VER-155008) or HSP90 inhibitor (17-AAG). (b) MTT assay to measure the cell viability of MCF-7 cells at 24 h after treated with VER-155008, 17-AAG and/or Apt-AuNP−GO (1.74 μg/mL in RPMI 1640 medium) combined with NIR illumination. (*$P < 0.05$).

compensatory expression of HSP70 or HSP90 in MCF-7 cells. In addition, the compensatory effect of an HSP90 inhibitor (17-AAG, 0.1 μM), strongly induces HSP70 expression, is consistent with the results reported previously by Chatterjee et al.[41] Once again, we suggest that an HSP70 inhibitor has the potential to serve as a better candidate than an HSP90 inhibitor for promoting the therapeutic efficiency of photothermal therapy for human breast cancer (Figures 4d and 5a).

In a proof-of-concept experiment concerning the inhibition of HSP70 function to enhance the therapeutic effect induced by photothermal therapy, MCF-7 cells were treated with Apt-AuNP−GO coupled with NIR illumination and/or HSP inhibitor. The temperatures of culture medium adjacent to

MCF-7 cells were about 53 °C in all treatment groups after continuous NIR illumination for 5 min (Figure S5, Supporting Information). In MTT assays (Figure 5b), we noted that the relative viability of MCF-7 cells cotreated with Apt-AuNP−GO (1.74 μg/mL) coupled with NIR laser irradiation and VER-155008 decreased to 39%, much lower than that of cells treated with Apt-AuNP−GO coupled with NIR laser irradiation (57%) and VER-155008 (96%). However, cotreatment of MCF-7 cells with Apt-AuNP−GO coupled with NIR laser irradiation and 17-AAG did not induce statistically significant changes in cell viability compared with the treatment of MCF-7 cells with Apt-AuNP−GO coupled with NIR laser irradiation. Our results revealed that the combined use of Apt-AuNP−GO and HSP70 inhibitor has a synergistic therapeutic effect and is more efficient than a single therapeutic agent for the treatment of breast cancer.

4. CONCLUSION

In summary, we unveil the therapeutic effects of Apt-AuNP−GO on MUC1-positive human breast cancer cells, which could be used for photothermal therapy. The Apt-AuNP−GO photothermal treatment resulted in the targeted inhibition of breast cancer MCF-7 cell growth by inducing apoptosis. In addition, the Apt-AuNP−GO was observed to possess an excellent NIR photothermal energy conversion capability and is able to induce a photothermal effect against breast cancer at ultralow concentration without inducing cell death in healthy cells. Furthermore, the absence of HSP70 protein induced by Apt-AuNP−GO with NIR illumination may result in irreversible cell death. Therefore, the degree and duration of HSP70 protein expression are correlated with the therapeutic effects against breast cancer for photothermal therapy. A synergistic therapeutic effect was observed when using hyperthermia and HSP70 inhibition, resulting in a significant enhancement of breast cancer cell death. The HSP70 inhibitor, which did not induce any compensatory effects, is a better chemo-phototherapeutic agent than the HSP90 inhibitor in combating human breast cancer. Our strategy could be extended to the construction of HSP70 inhibitor-loaded Apt-AuNP−GO for the synergistic therapeutic treatment of breast cancer because the inhibitor-loaded material may selectively deliver both heat and the HSP70 inhibitor to breast cancer cells and further improve therapeutic effectiveness with minimal side effects.

■ ASSOCIATED CONTENT

Ⓢ Supporting Information

Preparation and characterization procedures of GO nanosheets, Apt-AuNPs, and Apt-AuNP−GO; photothermal conversion efficiency and agarose gel separation of Apt-AuNP−GO; results obtained for Agarose gel separation, TEM, UV−vis absorption spectra, Raman spectra, Western blot image, immunolabeling stain image, and photothermal effect. This material is available free of charge via the Internet at http://pubs.acs.org.

■ AUTHOR INFORMATION

Corresponding Authors
*Tel: 86-512-6287-2586. Fax: 86-512-6260-3079. E-mail: jhlin2012@sinano.ac.cn.
*Tel: 886-2-2462-2192 ext. 5517. Fax: 886-2-2462-2320. E-mail: huanging@ntou.edu.tw.

REFERENCES

(1) Bray, F.; Ren, J. S.; Masuyer, E.; Ferlay, J. Global Estimates of Cancer Prevalence for 27 Sites in the Adult Population in 2008. *Int. J. Cancer* **2013**, *132*, 1133−1145.

(2) Ferlay, J., Soerjomataram, I., Ervik, M., Dikshit, R., Eser, S., Mathers, C., Rebelo, M., Parkin, D. M., Forman, D., Bray, F.; GLOBOCAN 2012 v1.0: Cancer Incidence and Mortality Worldwide. CancerBase No. 11. International Agency for Research on Cancer, World Health Organization: Lyon, France; 2013.

(3) Wu, P.; Gao, Y.; Zhang, H.; Cai, C. Aptamer-Guided Silver-Gold Bimetallic Nanostructures with Highly Active Surface-Enhanced Raman Scattering for Specific Detection and Near-Infrared Photothermal Therapy of Human Breast Cancer Cells. *Anal. Chem.* **2012**, *84*, 7692−7699.

(4) Yin, D.; Li, Y.; Lin, H.; Guo, B.; Du, Y.; Li, X.; Jia, H.; Zhao, X.; Tang, J.; Zhang, L. Functional Graphene Oxide as a Plasmid-Based Stat3 SiRNA Carrier Inhibits Mouse Malignant Melanoma Growth in Vivo. *Nanotechnology* **2013**, *24*, 105102.

(5) Chen, Y.-W.; Chen, P.-J.; Hu, S.-H.; Chen, I. W.; Chen, S.-Y. NIR-Triggered Synergic Photo-Chemothermal Therapy Delivered by Reduced Graphene Oxide/Carbon/Mesoporous Silica Nanocookies. *Adv. Funct. Mater.* **2013**, *24*, 451−459.

(6) Xu, C.; Yang, D.; Mei, L.; Li, Q.; Zhu, H.; Wang, T. Targeting Chemophotothermal Therapy of Hepatoma by Gold Nanorods/ Graphene Oxide Core/Shell Nanocomposites. *ACS Appl. Mater. Interfaces* **2013**, *5*, 12911−12920.

(7) Zedan, A. F.; Moussa, S.; Terner, J.; Atkinson, G.; El-Shall, M. S. Ultrasmall Gold Nanoparticles Anchored to Graphene and Enhanced Photothermal Effects by Laser Irradiation of Gold Nanostructures in Graphene Oxide Solutions. *ACS Nano* **2013**, *7*, 627−636.

(8) Cheng, L.; Liu, J.; Gu, X.; Gong, H.; Shi, X.; Liu, T.; Wang, C.; Wang, X.; Liu, G.; Xing, H.; Bu, W.; Sun, B.; Liu, Z. PEGylated WS_2 Nanosheets as a Multifunctional Theranostic Agent for in Vivo Dual-Modal CT/Photoacoustic Imaging Guided Photothermal Therapy. *Adv. Mater.* **2014**, *26*, 1886−1893.

(9) Wang, C.; Cheng, L.; Liu, Y.; Wang, X.; Ma, X.; Deng, Z.; Li, Y.; Liu, Z. Imaging-Guided pH-Sensitive Photodynamic Therapy Using Charge Reversible Upconversion Nanoparticles under Near-Infrared Light. *Adv. Funct. Mater.* **2013**, *23*, 3077−3086.

(10) Lu, F.; Popa, A.; Zhou, S.; Zhu, J. J.; Samia, A. C. S. Iron Oxide-Loaded Hollow Mesoporous Silica Nanocapsules for Controlled Drug Release and Hyperthermia. *Chem. Commun.* **2013**, *49*, 11436−11438.

(11) Zhang, F.; Braun, G. B.; Pallaoro, A.; Zhang, Y.; Shi, Y.; Cui, D.; Moskovits, M.; Zhao, D.; Stucky, G. D. Mesoporous Multifunctional Upconversion Luminescent and Magnetic "Nanorattle" Materials for Targeted Chemotherapy. *Nano Lett.* **2012**, *12*, 61−67.

(12) Luo, Y.-L.; Shiao, Y.-S.; Huang, Y.-F. Release of Photoactivatable Drugs from Plasmonic Nanoparticles for Targeted Cancer Therapy. *ACS Nano* **2011**, *5*, 7796−7804.

(13) Overgaard, J. The Current and Potential Role of Hyperthermia in Radiotherapy. *Int. J. Radiat. Oncol. Biol. Phys.* **1989**, *16*, 535−549.

(14) Lepock, J. R. Cellular Effects of Hyperthermia: Relevance to the Minimum Dose for Thermal Damage. *Int. J. Hyperthermia* **2003**, *19*, 252−266.

(15) Ke, H.; Yue, X.; Wang, J.; Xing, S.; Zhang, Q.; Dai, Z.; Tian, J.; Wang, S.; Jin, Y. Gold Nanoshelled Liquid Perfluorocarbon Nanocapsules for Combined Dual Modal Ultrasound/CT Imaging and Photothermal Therapy of Cancer. *Small* **2014**, *10*, 1220−1227.

(16) Shen, S.; Kong, F.; Guo, X.; Wu, L.; Shen, H.; Xie, M.; Wang, X.; Jin, Y.; Ge, Y. CMCTS Stabilized Fe_3O_4 Particles with Extremely Low Toxicity as Highly Efficient Near-Infrared Photothermal Agents for in Vivo Tumor Ablation. *Nanoscale* **2013**, *5*, 8056−8066.

(17) Akhavan, O.; Ghaderi, E. Graphene Nanomesh Promises Extremely Efficient in Vivo Photothermal Therapy. *Small* **2013**, *9*, 3593−3601.

(18) Antaris, A. L.; Robinson, J. T.; Yaghi, O. K.; Hong, G.; Diao, S.; Luong, R.; Dai, H. Ultra-Low Doses of Chirality Sorted (6,5) Carbon Nanotubes for Simultaneous Tumor Imaging and Photothermal Therapy. *ACS Nano* **2013**, *7*, 3644−3652.

(19) Cole, J. R.; Mirin, N. A.; Knight, M. W.; Goodrich, G. P.; Halas, N. J. Photothermal Efficiencies of Nanoshells and Nanorods for Clinical Therapeutic Applications. *J. Phys. Chem. C* **2009**, *113*, 12090−12094.

(20) Dreaden, E. C.; Mackey, M. A.; Huang, X.; Kanga, B.; El-Sayed, M. A. Beating Cancer in Multiple Ways Using Nanogold Chem. *Soc. Rev.* **2011**, *40*, 3391−3404.

(21) Robinson, J. T.; Tabakman, S. M.; Liang, Y.; Wang, H.; Sanchez Casalongue, H.; Vinh, D.; Dai, H. Ultrasmall Reduced Graphene Oxide with High Near-Infrared Absorbance for Photothermal Therapy. *J. Am. Chem. Soc.* **2011**, *133*, 6825−6831.

(22) Zhou, K.; Zhu, Y.; Yang, X.; Li, C. One-Pot Preparation of Graphene/Fe_3O_4 Composites by a Solvothermal Reaction. *New J. Chem.* **2010**, *34*, 2950−2955.

(23) Kakran, M.; Sahoo, N. G.; Bao, H.; Pan, Y.; Li, L. Functionalized Graphene Oxide as Nanocarrier for Loading and Delivery of Ellagic Acid. *Curr. Med. Chem.* **2011**, *18*, 4503−4512.

(24) Shiang, Y. C.; Ou, C. M.; Chen, S. J.; Ou, T. Y.; Lin, H. J.; Huang, C. C.; Chang, H. T. Highly Efficient Inhibition of Human Immunodeficiency Virus Type 1 Reverse Transcriptase by Aptamers Functionalized Gold Nanoparticles. *Nanoscale* **2013**, *5*, 2756−2764.

(25) Zhang, Z.; Ali, M. M.; Eckert, M. A.; Kang, D. K.; Chen, Y. Y.; Sender, L. S.; Fruman, D. A.; Zhao, W. A Polyvalent Aptamer System for Targeted Drug Delivery. *Biomaterials* **2013**, *34*, 9728−9735.

(26) Barbas, A. S.; Mi, J.; Clary, B. M.; White, R. R. Aptamer Applications for Targeted Cancer Therapy. *Future Oncol.* **2010**, *6*, 1117−1126.

(27) Tan, L.; Neoh, K. G.; Kang, E. T.; Choe, W. S.; Su, X. Pegylated Anti-Muc1 Aptamer-Doxorubicin Complex for Targeted Drug Delivery to MCF7 Breast Cancer Cells. *Macromol. Biosci.* **2011**, *11*, 1331−1335.

(28) Gaemers, I. C.; Vos, H. L.; Volders, H. H.; van der Valk, S. W.; Hilkens, J. A Stat-Responsive Element in the Promoter of the Episialin/MUC1 Gene Is Involved in Its Overexpression in Carcinoma Cells. *J. Biol. Chem.* **2001**, *276*, 6191−6199.

(29) Walsh, M. D.; Luckie, S. M.; Cummings, M. C.; Antalis, T. M.; McGuckin, M. A. Heterogeneity of MUC1 Expression by Human Breast Carcinoma Cell Lines in Vivo and in Vitro. *Breast Cancer Res. Treat.* **1999**, *58*, 255−266.

(30) Hattrup, C. L.; Gendler, S. J. MUC1 Alters Oncogenic Events and Transcription in Human Breast Cancer Cells. *Breast Cancer Res.* **2006**, *8*, R37.

(31) Mosser, D. D.; Morimoto, R. I. Molecular Chaperones and the Stress of Oncogenesis. *Oncogene* **2004**, *23*, 2907−2918.

(32) Kim, L. S.; Kim, J. H. Heat Shock Protein as Molecular Targets for Breast Cancer Therapeutics. *J. Breast Cancer* **2011**, *14*, 167−174.

(33) Siebelt, M.; Jahr, H.; Groen, H. C.; Sandker, M.; Waarsing, J. H.; Kops, N.; Muller, C.; van Eden, W.; de Jong, M.; Weinans, H. HSP90 Inhibition Protects against Biomechanically Induced Osteoarthritis in Rats. *Arthritis Rheumatol.* **2013**, *65*, 2102−2112.

(34) Jego, G.; Hazoume, A.; Seigneuric, R.; Garrido, C. Targeting Heat Shock Proteins in Cancer. *Cancer Lett.* **2013**, *332*, 275−285.

(35) Mosser, D. D.; Caron, A. W.; Bourget, L.; Denis-Larose, C.; Massie, B. Role of the Human Heat Shock Protein HSP70 in Protection against Stress-Induced Apoptosis. *Mol. Cell. Biol.* **1997**, *17*, 5317−5327.

(36) Moseley, P. L. Heat Shock Proteins and Heat Adaptation of the Whole Organism. *J. Appl. Physiol.* **1997**, *83*, 1413−1417.

(37) Huang, H. C.; Yang, Y.; Nanda, A.; Koria, P.; Rege, K. Synergistic Administration of Photothermal Therapy and Chemo-

therapy to Cancer Cells Using Polypeptide-Based Degradable Plasmonic Matrices. *Nanomedicine (London, U. K.)* **2011**, *6*, 459−473.

(38) Ito, A.; Saito, H.; Mitobe, K.; Minamiya, Y.; Takahashi, N.; Maruyama, K.; Motoyama, S.; Katayose, Y.; Ogawa, J. Inhibition of Heat Shock Protein 90 Sensitizes Melanoma Cells to Thermosensitive Ferromagnetic Particle-Mediated Hyperthermia with Low Curie Temperature. *Cancer Sci.* **2009**, *100*, 558−564.

(39) Milanovic, D.; Firat, E.; Grosu, A. L.; Niedermann, G. Increased Radiosensitivity and Radiothermosensitivity of Human Pancreatic MIA PaCa-2 and U251 Glioblastoma Cell Lines Treated with the Novel HSP90 Inhibitor NVP-HSP990. *Radiat. Oncol.* **2013**, *8*, 42.

(40) Massey, A. J.; Williamson, D. S.; Browne, H.; Murray, J. B.; Dokurno, P.; Shaw, T.; Macias, A. T.; Daniels, Z.; Geoffroy, S.; Dopson, M.; Lavan, P.; Matassova, N.; Francis, G. L.; Graham, C. J.; Parsons, R.; Wang, Y.; Padfield, A.; Comer, M.; Drysdale, M. J.; Wood, M. A Novel, Small Molecule Inhibitor of HSC70/HSP70 Potentiates HSP90 Inhibitor Induced Apoptosis in HCT116 Colon Carcinoma Cells. *Cancer Chemother. Pharmacol.* **2010**, *66*, 535−545.

(41) Chatterjee, M.; Andrulis, M.; Stuhmer, T.; Muller, E.; Hofmann, C.; Steinbrunn, T.; Heimberger, T.; Schraud, H.; Kressmann, S.; Einsele, H.; Bargou, R. C. The PI3K/Akt Signaling Pathway Regulates the Expression of HSP70, Which Critically Contributes to HSP90-Chaperone Function and Tumor Cell Survival in Multiple Myeloma. *Haematologica* **2013**, *98*, 1132−1141.

(42) Guo, F.; Rocha, K.; Bali, P.; Pranpat, M.; Fiskus, W.; Boyapalle, S.; Kumaraswamy, S.; Balasis, M.; Greedy, B.; Armitage, E. S.; Lawrence, N.; Bhalla, K. Abrogation of Heat Shock Protein 70 Induction as a Strategy to Increase Antileukemia Activity of Heat Shock Protein 90 Inhibitor 17-Allylamino-Demethoxy Geldanamycin. *Cancer Res.* **2005**, *65*, 10536−10544.

(43) Lanneau, D.; Brunet, M.; Frisan, E.; Solary, E.; Fontenay, M.; Garrido, C. Heat Shock Proteins: Essential Proteins for Apoptosis Regulation. *J. Cell. Mol. Med.* **2008**, *12*, 743−761.

(44) Hummers, W. S.; Offeman, R. E. Preparation of Graphitic Oxide. *J. Am. Chem. Soc.* **1958**, *80*, 1339−1339.

(45) Kudin, K. N.; Ozbas, B.; Schniepp, H. C.; Prud'homme, R. K.; Aksay, I. A.; Car, R. Raman Spectra of Graphite Oxide and Functionalized Graphene Sheets. *Nano Lett.* **2008**, *8*, 36−41.

(46) Manani, G.; Morris, M.; Caudle, S.; Wanekaya, A.; Mugweru, A. Electrocatalytic Oxidation of Propranol Using Microwave Synthesized Graphene Decorated with Gold Nanoparticles and Single Walled Carbon Nanotubes. Chem. *Mater. Res.* **2013**, *3*, 39−48.

(47) Marcano, D. C.; Kosynkin, D. V.; Berlin, J. M.; Sinitskii, A.; Sun, Z.; Slesarev, A.; Alemany, L. B.; Lu, W.; Tour, J. M. Improved Synthesis of Graphene Oxide. *ACS Nano* **2010**, *4*, 4806−4814.

(48) Mucic, R. C.; Storhoff, J. J.; Mirkin, C. A.; Letsinger, R. L. DNA-Directed Synthesis of Binary Nanoparticle Network Materials. *J. Am. Chem. Soc.* **1998**, *120*, 12674−12675.

(49) Liua, Y.; Liua, C. Y.; Liua, Y. Investigation on Fluorescence Quenching of Dyes by Graphite Oxide and Graphene. *Appl. Surf. Sci.* **2011**, *257*, 5513−5518.

(50) Wang, Y.; Wang, H.; Liu, D.; Song, S.; Wang, X.; Zhang, H. Graphene Oxide Covalently Grafted Upconversion Nanoparticles for Combined NIR Mediated Imaging and Photothermal/Photodynamic Cancer Therapy. *Biomaterials* **2013**, *34*, 7715−7724.

(51) Qin, X. C.; Guo, Z. Y.; Liu, Z. M.; Zhang, W.; Wan, M. M.; Yang, B. W. Folic Acid-Conjugated Graphene Oxide for Cancer Targeted Chemo-Photothermal Therapy. *J. Photochem. Photobiol., B* **2013**, *120*, 156−162.

(52) Lim, D. K.; Barhoumi, A.; Wylie, R. G.; Reznor, G.; Langer, R. S.; Kohane, D. S. Enhanced Photothermal Effect of Plasmonic Nanoparticles Coated with Reduced Graphene Oxide. *Nano Lett.* **2013**, *13*, 4075−4079.

(53) Abdelsayed, V.; Moussa, S.; Hassan, H. M.; Aluri, H. S.; Collinson, M. M.; El-Shall, M. S. Photothermal Deoxygenation of Graphite Oxide with Laser Excitation in Solution and Graphene-Aided Increase in Water Temperature. *J. Phys. Chem. Lett.* **2010**, *1*, 2804−2809.

(54) Kroll, A.; Pillukat, M. H.; Hahn, D.; Schnekenburger, J. Interference of Engineered Nanoparticles with in Vitro Toxicity Assays. *Arch. Toxicol.* **2012**, *86*, 1123−1136.

(55) Huang, J.; Zong, C.; Shen, H.; Liu, M.; Chen, B.; Ren, B.; Zhang, Z. Mechanism of Cellular Uptake of Graphene Oxide Studied by Surface-Enhanced Raman Spectroscopy. *Small* **2012**, *8*, 2577−2584.

(56) Elmore, S. Apoptosis: A Review of Programmed Cell Death. *Toxicol. Pathol.* **2007**, *35*, 495−516.

(57) Schmitt, E.; Gehrmann, M.; Brunet, M.; Multhoff, G.; Garrido, C. Intracellular and Extracellular Functions of Heat Shock Proteins: Repercussions in Cancer Therapy. *J. Leukocyte Biol.* **2007**, *81*, 15−27.